

DC electrodeposition of Mn–Co alloys on stainless steels for SOFC interconnect application

Junwei Wu^a, Yinglu Jiang^a, Christopher Johnson^b, Xingbo Liu^{a,*}

^a Mechanical and Aerospace Engineering Department, West Virginia University, Morgantown, WV 26506, USA

^b National Energy Technology Laboratory, Department of Energy, Morgantown, WV 26507, USA

Received 1 November 2007; received in revised form 14 November 2007; accepted 15 November 2007

Available online 9 January 2008

Abstract

High conductivity coatings that resist oxide scale growth and reduce chromium evaporation are needed to make stainless steel interconnect materials viable for long-term stable operation of solid oxide fuel cells (SOFC). $Mn_{1.5}Co_{1.5}O_4$ spinel is one of the most promising coatings for interconnect application because of its high conductivity, good chromium retention capability, as well as good CTE match to ferritic stainless steels. Mn–Co electrodeposition followed by oxidation is potentially a low cost method for fabrication of $(Mn,Co)_3O_4$ spinel coatings. This work looks at the co-deposition of Mn–Co alloys for this application. As a guide to optimize the deposition process, characterizations of the cathodic reactions and reaction potentials are done using polarization curves. It was found that as cobalt concentration was varied that the alloy composition became richer in cobalt, indicating that the deposition is regular co-deposition process. It was also found that at 0.05 M Co concentration in excess gluconate the Mn–Co alloys composition could be tuned by varying the current density. Coatings with Mn–Co around 1:1 could be obtained at a current density of 250 mA/cm². However, the higher potential increased hydrogen production making the films more porous. Oxidation of the alloy coatings showed that much of the porosities could be eliminated during oxidation. It was found in a number of samples that fully dense coatings were obtained. The composition of the oxidized coating was found to become enriched in Mn, possibly due to the Mn fast diffusion from the substrate.

© 2007 Elsevier B.V. All rights reserved.

Keywords: Interconnect; Manganese; Cobalt; SOFC; Electrodeposition

1. Introduction

The solid oxide fuel cells (SOFCs) are promising candidates for future energy conversion systems because they have higher energy conversion efficiency than conventional heat engine systems and other types of fuel cells. Interconnects are in contact with both electrodes and act as electrical connection in a SOFC stacks, and thus there are a number of requirements they must meet. They must exhibit long-term stability in both oxidizing (air side) and reducing (fuel side) environment, good conductivity, and good CTE match with other ceramic components [1]. Decreasing the operation temperature of SOFC to between 600 and 800 °C enables the use of cheap metallic interconnects materials such as stainless steel or other chromia-forming alloys [2,3].

However, bare metal does not remain stable after long time operation at high temperature [4] because of continued scale growth and high volatility of Cr(VI), which can contaminate electrolyte and cathode, and cause degradation of SOFC performance. Even newly developed Fe–Cr–Mn [5] alloys, Crofer 22 APU (ThyssenKrupp VDM) and ZMG232 (Hitachi Metals), that form $(Mn,Cr)_3O_4$ spinel as the top scale layer do not eliminate Cr volatility completely [1].

One of the most effective approaches to improve the interconnect properties is to apply surface coatings to provide better conductivity, reduced scale growth and Cr volatility. Recently, cobalt and containing spinels, such as MOCVD deposited Co_3O_4 [6], $MnCo_2O_4$ by slurry coating and electroplating followed by oxidation [7,8], electroplating and PVD coatings of pure cobalt [9,10], have shown promising results for SOFC applications due to good conductivity and improved chromium retention capabilities, nevertheless, $Mn_{1.5}Co_{1.5}O_4$ spinel is the most promising, because of its high conductivity (60 S/cm at

* Corresponding author.

E-mail address: xingbo.liu@mail.wvu.edu (X. Liu).

800 °C) and good CTE ($11.5 \times 10^{-6}/\text{K}$, 20–800 °C) match with ferritic stainless steel and SOFC cathode materials (LSM). Long-term high temperature tests show little or no chromium diffusion through the coating layers after 6 months [11,12].

The $\text{Mn}_{1.5}\text{Co}_{1.5}\text{O}_4$ spinel has been applied to metallic interconnect materials by means of slurry coating, screen printing, and PVD. Electroplating of alloys, followed by controlled oxidation offers an alternative method of fabricating spinel coatings, which have been successfully proven previously [8,13]. The advantages of electroplating include low cost, being capable of coating complex geometries, and direct deposition of an alloy may not require any additional processing steps the oxidation can be part of the initial stack start up. During this process, well adhered, compact spinel coatings are produced.

In the past, electrodeposition of Mn–Co alloys has been carried out by Abd El Rehim et al. [14], the author has attempted to repeat the experiments, but were not successful and other literature gave different summary about the Mn percentage change with current density [15]. On the other hand, some other researchers used very dilute more noble metallic salt solutions [16], which is only practical for lab experimental. In this work, to improve the cost-effectiveness, and to make the solution practical for mass production, Mn–Co alloy co-deposition was obtained by electrodeposition based on SS430 in solutions with Mn–Co ratio of 5. The effect of current density and the addition of some additives on surface morphology and Mn–Co ratio in the coatings, as well as a better understanding of the deposition processes as characterized by polarization curves are reported.

2. Experimental

2.1. Electrolytes

All of the electrodeposition experiments were carried out in 1 L electrolytes prepared with deionized water. All chemicals used were of laboratory reagent grade from Alfa Aesar and Bioworld. The pH of electrolytes was adjusted using either ammonia hydroxide or 20 vol.% H_2SO_4 .

The electrolyte used in the initial electrodeposition trials was a simple solution from reference [14] but with a different concentration, containing 0.01 M CoSO_4 , 0.50 M MnSO_4 , and 0.50 M H_3BO_3 , and 0.70 M gluconate. The pH was adjusted to 3.0. After each electrodeposition, the pH was measured and readjusted to the original value.

A one-compartment cell was employed for DC electrodeposition. The preparation of electrolyte was similar to previous plating work [17]. Boric acid (pH buffer) and sodium gluconate (chelating agent), were then added with magnetic stirrer agitation. Once these chemicals were completely dissolved, cobalt sulfate was added slowly with continued agitation for 30 min. The solution was then kept standing for 24 h to allow the chelating reaction between cobalt(II) species and gluconate to approach equilibrium. This was followed by the addition of manganese sulfate and ammonium sulfate together with agitation. The pH of the solution was then measured and adjusted to the values specified. Finally the solution was topped up to the correct working volume.

Table 1
Composition of SS430 (wt.%)

Mn	Si	Cr	Ni	Co	W	Al	Fe	C	S
0.48	<0.01	17	0.06	<0.01	0.015	0.012	82.28	0.0482	0.002

The counter electrode was a platinum plate placed in the same compartment of working electrode. Steel plates with surface area a little larger than 1 cm^2 the edge is covered by Teflon to reduce edge effect [18] and exposure area was exactly 1 cm^2 .

2.2. Substrate preparation

SS 430 was chosen as the substrate due to its low cost and simple processing method. The substrate composition is shown in Table 1. The substrates were first mechanically polished with various grades of silicon carbide papers up to 2400 grit. For degreasing, the substrates were ultrasonically degreased in acetone for 10 min. After rinsing in running tap water and then ultrasonically cleaned in deionized water and ethanol for 2 min each. At last, the substrates were pickled in mixed 5% nitric and 25% hydrochloric acid just before use.

2.3. Electrochemical test

Cathodic potentiodynamic behavior of the various electrolytes were determined using linear sweep voltammetry, with a scan rate of 5 mV s^{-1} , and in a potential range from 0.1 V vs. open circuit potential (OCP) to -2.5 V vs. OCP. A potentiostat/galvanostat (Solartron 1287) controlled by a computer was used for all the electrochemical measurements. All potentials were measured relative to a saturated calomel electrode (SCE).

2.4. Optimization of electrodeposition process

Simple electrolyte solutions were used to perform fundamental experiments to confirm the range of deposition parameters for the Co and Mn cations. The solutions used contained 0.01 M CoSO_4 , 0.50 M MnSO_4 , and 0.50 M H_3BO_3 , 0.70 M sodium gluconate, and the pH was adjusted to 3.0. Considering the much more negative deposition potential of Mn, longer time (20 min) was applied for each experiment to compensate for H_2 formation.

After the preliminary results were obtained, electrolyte composition was adjusted slightly. In addition, the effect of chelating agent amount, current density and cobalt concentration were studied.

3. Results and discussion

3.1. Potentiodynamic behavior

Since cobalt is the nobler metal in this system, the concentration ratio of Co to Mn ions in the electrolyte has to be much lower than the ratio required in the alloy. The standard electrode potential of Co is -0.277 V vs. standard hydrogen electrode (SHE) [19] and that of Mn is -1.180 V vs. SHE [20], which means that

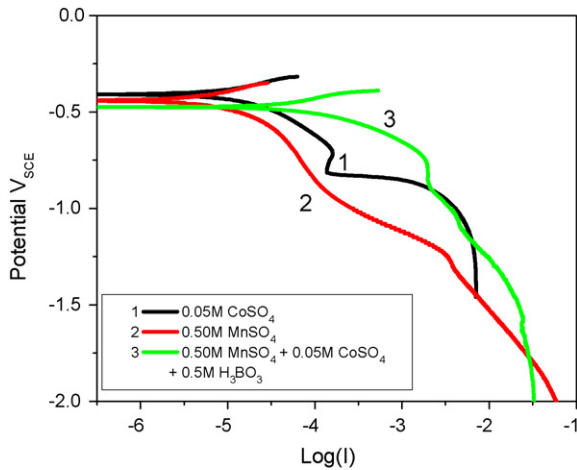


Fig. 1. Potentiodynamic behavior of Co, Mn, and Mn–Sn solutions with H_3BO_3 .

their deposition potentials are far apart for noncomplexed ions, making the co-deposition difficult from a simple sulfate solution of Mn and Co ions.

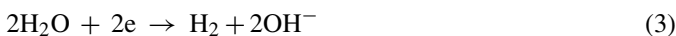
In order to understand the influence of each component of the solution, polarization measurements were first performed in solutions of 0.50 M MnSO_4 , 0.05 M CoSO_4 , 0.50 M $\text{MnSO}_4 + 0.05 \text{ M CoSO}_4 + 0.50 \text{ M H}_3\text{BO}_3$. Fig. 1 shows the polarization curves for a 0.05 M CoSO_4 solution, a 0.50 M MnSO_4 solution, and a solution containing 0.05 M CoSO_4 , 0.50 M MnSO_4 and 0.50 M H_3BO_3 . Two plateaus were observed in the 0.05 M CoSO_4 solution, the first corresponds to the limiting current density of reaction 1 below.



This reaction tends to increase the local pH near the sample surface. With the further increase of current density, Co^{2+} deposition begins to occur at -0.815 V vs. SCE , the reaction is



In a solution of 0.50 M $\text{MnSO}_4 + 0.05 \text{ M CoSO}_4 + 0.50 \text{ M H}_3\text{BO}_3$, the limiting current density of Eq. (1) becomes much higher due to the effect of H_3BO_3 buffer, which helps to maintain the local pH value near the substrate surface during deposition. Additionally, Eq. (2) begins to occur at $\sim 0.880 \text{ V vs. SCE}$. The negative shift of the potential is due to the chelating effect of H_3BO_3 . By further increasing the current density, the water splitting reaction may occur around $\sim 1.10 \text{ V}_{\text{SCE}}$, which will also increase the local pH value.



However, Eq. (3) is not obvious in pure 0.05 M CoSO_4 system, probably due to the overlap with strong Co^{2+} reduction reaction. In 0.50 M MnSO_4 solution, the slope of at $-1.0 \text{ V}_{\text{SCE}}$ is due to the onset of Eq. (3). Further increase in current density results in the other main deposition reaction (4) occurring around $\sim 1.5 \text{ V}_{\text{SCE}}$.

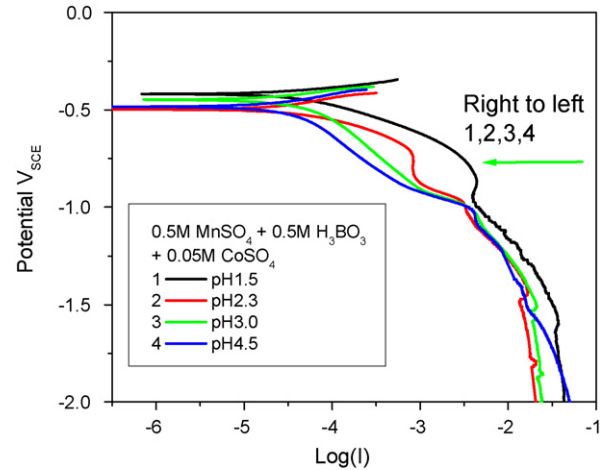


Fig. 2. Potentiodynamic behavior of $\text{MnSO}_4 + \text{CoSO}_4 + \text{H}_3\text{BO}_3$ based solutions with various pH values.

When current density is very high, the buffering capability of H_3BO_3 may not be enough to maintain local pH, and thus $\text{Mn}(\text{OH})_2$ or $\text{Co}(\text{OH})_2$, or both will form. Therefore, it is necessary to study pH effect on co-deposition. The effect of pH value for a 0.5 M $\text{MnSO}_4 + 0.05 \text{ M CoSO}_4 + 0.5 \text{ M H}_3\text{BO}_3$ solution were conducted at 1.5, 2.3, 3.0 and 4.5, and is shown in Fig. 2. At pH 1.5 solutions, reaction limit of H^+ is much higher, which implies more H_2 bubble will form during deposition, therefore, much higher porosity may be expected in deposition layer. Co^{2+} reduction begins to take place at $-0.95 \text{ V}_{\text{SCE}}$, and from pH value range from 2.3 to 4.5, there is no obvious difference in Co^{2+} deposition potential. At pH of 3.0 and 4.5, two clear plateaus for reactions 1 and 2 are also not present. On the other hand, variation of pH value does not change the Mn^{2+} reduction potential significantly, all of them begin to occur at $1.45\text{--}1.55 \text{ V}_{\text{SCE}}$.

Fig. 3 displays cathodic potentiodynamic behavior of solutions with different Co^{2+} concentrations. There is no obvious Co^{2+} reduction peak in 0.01 M Co^{2+} solution, due to the weak

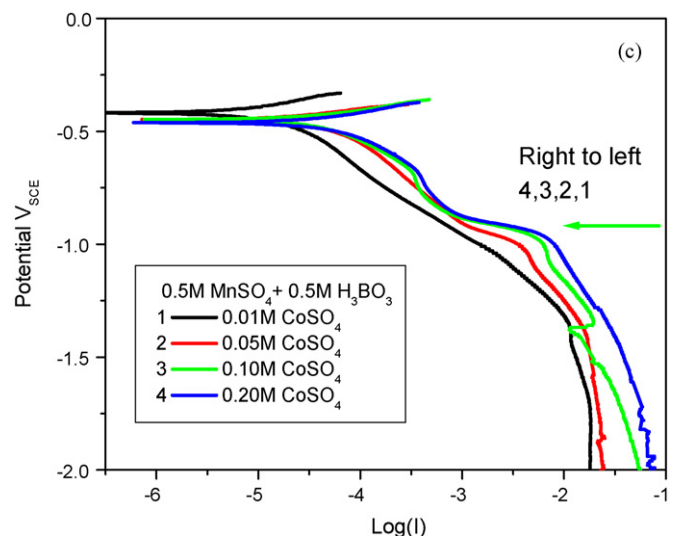


Fig. 3. Potentiodynamic behavior of MnSO_4 and H_3BO_3 based solutions with various CoSO_4 concentrations.

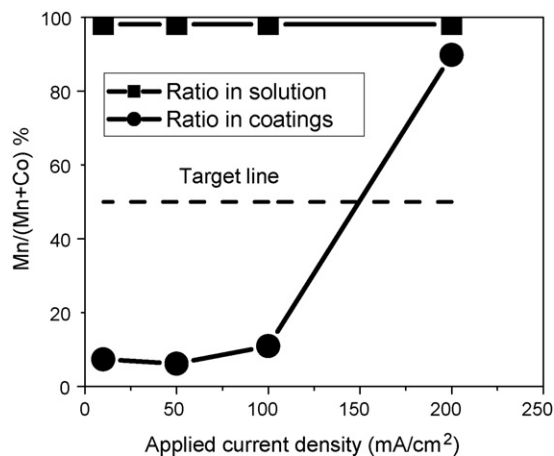


Fig. 4. Ratio of manganese with different current density (the result at 200 mA/cm² is the coating after being sonicated).

chelating effect of boric acid, which can reduce the free Co²⁺. As Co²⁺ concentration increases, a clear Co²⁺ plateau becomes apparent, and the plateau width increases with Co²⁺ concentration, which implies that H₃BO₃ has a much smaller chelating effect. This is also consistent with the Mn–Co co-deposition being regular co-deposition.

3.2. Preliminary electrodeposition

Alloy deposition via electro-plating for systems containing one or more of the nobler metals, such as Mn–Sn [15], Mn–Cu [18], often use very trace amounts of the noble metal ions in solution to bring the deposition potentials closer and increase the gap between deposition limiting current densities, which are similar to Mn–Co co-deposition. The Mn–Co deposition potentials differ considerably, implying the need for preliminary deposition experiments in dilute Co solutions. In the preliminary experiments, the solution used contained 0.01 M CoSO₄, 0.50 M MnSO₄, and 0.50 M H₃BO₃, 0.70 M sodium gluconate. Fig. 4 shows the Mn content in the coatings as a function of current densities, 10, 50, 100, and 200 mA/cm². No significant Mn% change was obtained from 10 to 100 mA/cm² and oxy-

gen content (O%) is less than 5%, however when the current density is increased further to 200 A/cm², over 20 at.% oxygen was detected by EDX in the coatings, and surface is spongy and porous, shown in Fig. 5(a). While EDX is typically not a quantitative method for light elements, this data qualitatively suggests the presence of MnO_x or Mn(OH)₂ in the coating. This is likely due to the local pH being increased out of the range that could be controlled by the pH buffer at 200 mA/cm². In order to observe the real morphology, the coating was sonicated in DI water for 2 min to remove the hydroxide, and the obvious morphology change was observed as shown in Fig. 5(b). Clearly, a more particulate structure with irregular particles packed together is visible. EDS confirmed that oxygen content is reduced to 3%, accordingly most hydroxide has been removed, and relative Mn content increased up to 93%.

For SOFC interconnect applications, it is likely that micron thicknesses will be necessary to allow the coatings to withstand 40,000 h of continuous operation. For example, in Mn_{1.5}Co_{1.5}O₄ coatings [11,12], coating thicknesses of 10 μm have been utilized, for the MnCo₂O₄ spinel thicknesses of more than 50 μm has been attempted [8]. However, formation of hydroxide makes it impossible to obtain thick coatings. More pH buffer may be capable of preventing Mn(OH)₂ production during deposition. (NH₄)₂SO₄ is also a commonly used pH buffer in the Mn alloys deposition solutions, and it has the added benefit of improving the conductivity of the electrolyte. On the other hand, as mentioned in one case [17], the disadvantage of dilute more noble metal solutions is detrimental, because electrolyte may become depleted and lose its chemical balance in a short electroplating time period, necessitating a large volume of electrolyte and very strict control of plating parameters.

Therefore, 0.5 M MnSO₄ + 0.10 M CoSO₄ + 1.0 M H₃BO₃ + 0.7 M Gluconate + 0.1 M (NH₄)₂SO₄ (pH 2.5) was chosen as the improved solution in the following deposition.

3.3. Effect of sodium gluconate content on the deposition

The amount of sodium gluconate concentration in the improved solutions is higher than the combined cation concentrations. In the Mn–Sn [15] and Mn–Cu [18] results, it

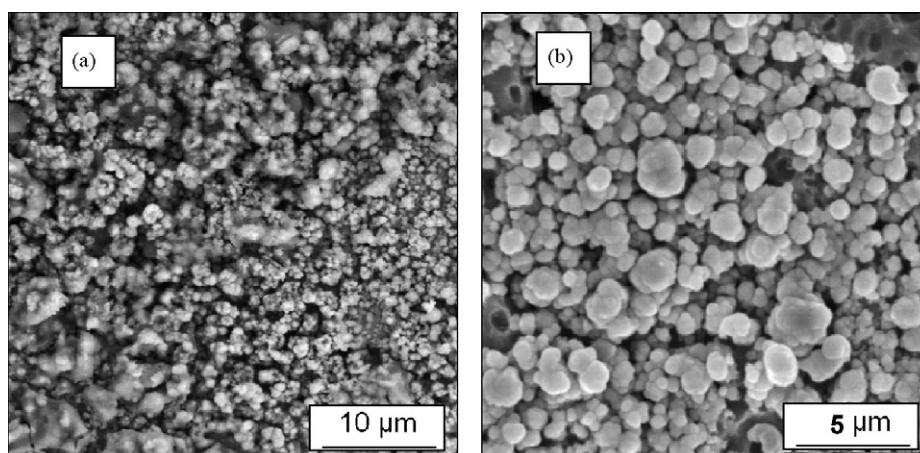


Fig. 5. SEM surface morphology of Mn–Co coating at 200 mA/cm² in Mn–Co = 50 solution. (a) As-deposited; (b) after being sonicated.

Table 2

Electrodeposition results in solution of 0.50 M MnSO₄ + 1.0 M H₃BO₃ + 0.10 M (NH₄)₂SO₄ (pH 2.5) with different gluconate at different current densities

	0.20 M gluconate	0.40 M gluconate	0.70 M gluconate
100 mA/cm ²	Not continuous	Dense, Mn ₁₅ Co ₈₅	Dense, Mn ₁₄ Co ₈₆
150 mA/cm ²	Not continuous	Semi-dense, Mn ₁₉ Co ₈₁	Semi-dense, Mn ₁₉ Co ₈₁
200 mA/cm ²	–	Not continuous	Porous, Mn ₃₇ Co ₆₃

is reported that chelating agents preferentially chelate with more noble metals, so less chelating agents is needed for co-deposition. Therefore, to clarify what chelating level is needed for this system different amounts of chelating agents were studied in the electrolyte of 0.50 M MnSO₄ + 0.10 M CoSO₄ + 1.0 M H₃BO₃ + 0.10 M (NH₄)₂SO₄ with 0.20 M, 0.40 M.

The solutions with different sodium gluconate concentrations were studied at different current densities. 100, 150, and 200 mA/cm². SEM/EDX result for all the deposited surfaces after deposition are summarized in Table 2. Images of surface morphologies after deposition are displayed in Fig. 6. No continuous coatings were obtained in 0.20 M gluconate solution from 100 mA to 150 mA/cm², only isolated particles were deposited, and particle size increased from 100 mA to 150 mA/cm². Some cracks were found below the isolated particles, EDX shows high amount of manganese and oxygen, probably indicating the for-

mation of manganese hydroxide. When gluconate concentration was increased to 0.40 M, continuous coating could be obtained at 100 and 150 mA/cm², EDX results demonstrated that relative Mn ratio is less than 20%. While as current density was further increased to 200 mA/cm², the coating becomes non-continuous as in the 0.20 M sodium gluconate solutions at 150 mA/cm², some cracks were also observed below the isolated particles. When the gluconate was added to as high as 0.70 M, continuous coatings were deposited at all of three current densities, and relative Mn content increased up to 36%. Therefore, as can be summarized that formation of hydroxide will inhibit the deposition of continuous coatings, and high amount of sodium gluconate (0.70 M) will be beneficiary to get high Mn content and continuous coatings.

During deposition at different current densities, cell voltage (V vs. platinum) was monitored as a function of time

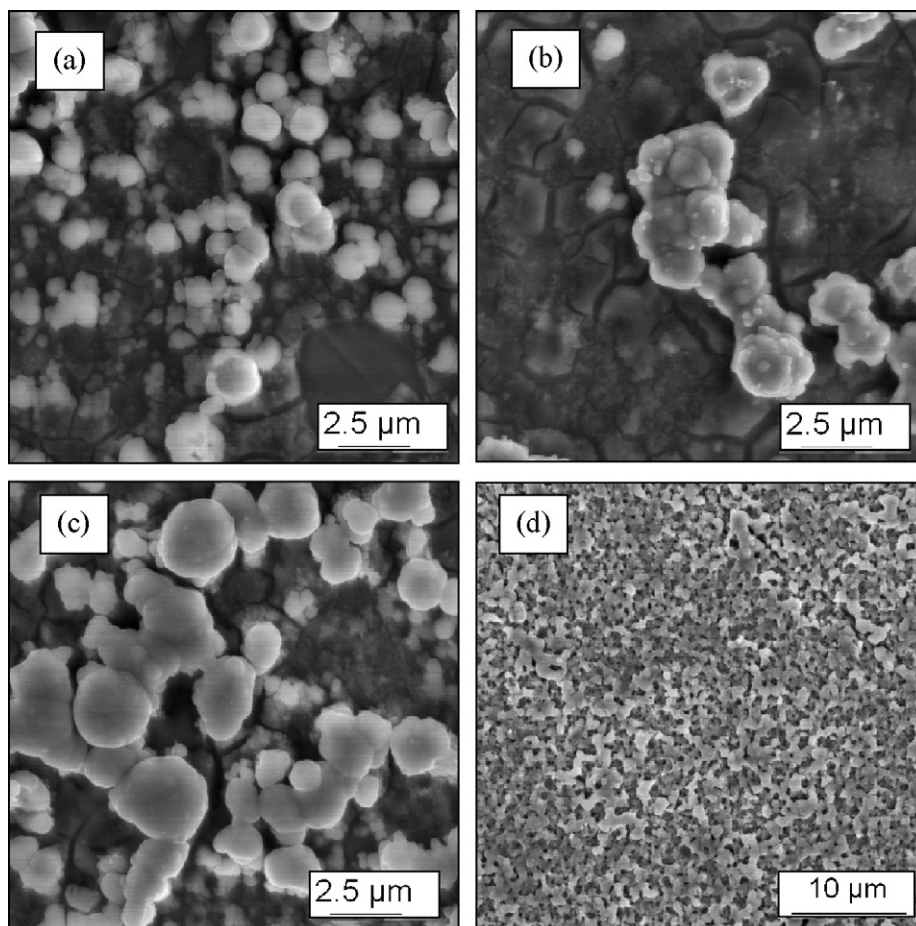


Fig. 6. Surface morphology of electrodeposition samples in the base solution of 0.50 M MnSO₄ + 0.10 M CoSO₄ + 1.0 M H₃BO₃ 0.1 M (NH₄)₂SO₄ (pH 2.5). (a) 100 mA/cm², 0.20 M gluconate; (b) 150 mA/cm², 0.20 M gluconate; (c) 200 mA/cm², 0.40 M gluconate; and (d) 200 mA/cm², 0.70 M gluconate.

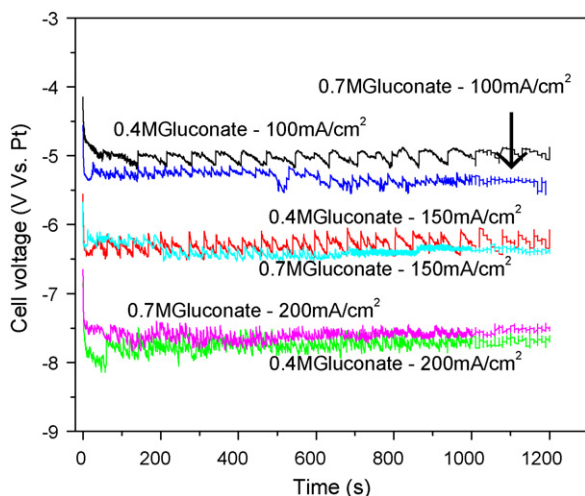


Fig. 7. Cell voltage change as a function of gluconate concentration, current density, and time.

(negative value is due to cathode), as shown in Fig. 7. Instability in the curves is likely due to hydrogen bubbles being formed on the substrate surface. At 100 mA/cm², voltage at 0.40 M is more negative than that of 0.70 M gluconate. At 150 mA/cm², voltage at 0.40 M is still more negative, but the difference is reduced, while at 200 mA/cm², the voltage at 0.70 M gluconate is becoming less negative than that of 0.40 M gluconate. The voltage trend change may be explained by a change in the surface species or morphology. At low current density, both the coatings are continuous and conductive, the higher amount of gluconate will chelate more free Co²⁺ and Mn²⁺ in the solution, and chelated ions always move slower than cations, therefore the resistance of the solution at 0.70 M gluconate is a little higher, and at the same current density, the voltage will be higher. When current density reaches 200 mA/cm², hydroxide is likely formed in the 0.40 M gluconate solution, which is not conductive and possesses high resistance. In 0.70 M gluconate solution at this same current density, the deposited film is continuous and conductive, so the voltage in 0.70 M gluconate is lower than that of 0.40 M gluconate at 200 mA/cm².

3.4. Effect of current density and cobalt concentration

Different amounts of CoSO₄ 0.05, 0.10 and 0.20 M in the solution of 0.50 M MnSO₄ + 1.0 M H₃BO₃ + 0.70 M gluconate + 0.1 M (NH₄)₂SO₄ (pH 2.5) were also studied with different current densities. Compositions obtained by EDX are shown in Fig. 8, which displays relative Mn% of coatings increases with current density in different cobalt concentration solutions. Mn% is still very low at 100 and 150 mA/cm², less than 20%. When further increasing current density, approximately 50% Mn coatings can be obtained in 0.05 and 0.10 M CoSO₄ solutions at 250 mA/cm². For Mn_{1.5}Co_{1.5}O₄ fabricated by other methods [11,12], achieving the correct spinel composition/phase depends strongly on the ratio of precursors, and thus our target precursor is a 50% alloy composition. At current density of 100 and 150 mA/cm², the Mn% in the coatings is very

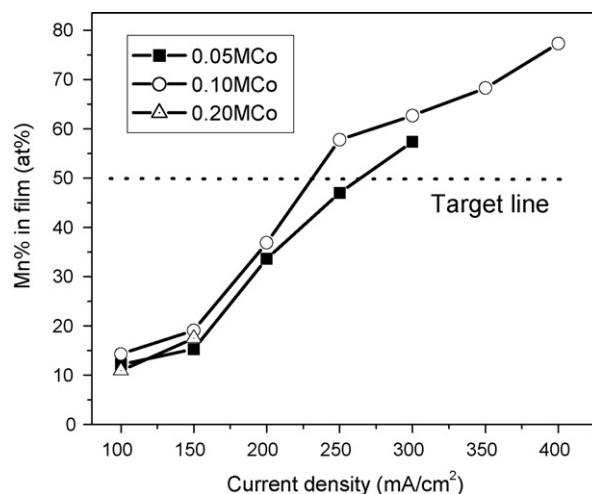


Fig. 8. Surface composition of coatings with different current density in solution of 0.50 M MnSO₄ + 1.0 M H₃BO₃ + 0.70 M gluconate + 0.10 M (NH₄)₂SO₄ (pH 2.5).

close in all three solutions. The Mn content increases with current density, however, in the 0.20 M CoSO₄ solutions, Mn(OH)₂ will be formed at 200 mA/cm², which inhibits further deposition of coatings, therefore the coatings are not continuous, and EDX results are not available.

SEM surface morphologies are displayed in Fig. 9 of the coatings in 0.05 M CoSO₄ solutions. At current density as low as 100 mA/cm², the coating is uniform, low porosity, and made up of small particles. With increase to 150 mA/cm², the coating particle sizes increase a little, and with very low porosity. As further increase to 200, 250, 300 mA/cm², the particle size does not change, however, the porosity increases significantly. The trends are the same as that in the 0.10 M CoSO₄ solution.

Current efficiency is demonstrated in Fig. 10 as a function of current density and cobalt concentration. With increase of cobalt concentration, efficiency increases significantly at 100 and 150 mA/cm², and as further increased to 200 mA/cm² or higher, all efficiencies remain very low and very close. During Mn–Co cathodic co-depositions, four reactions could occur according to potentiodynamic polarization results. Reactions (1) and (3) result in no deposition and waste current, at high current densities, more hydrogen bubbles are produced, which results in lower current efficiency, consistent with the surface morphologies change with current densities. At low current densities, low porosities were obtained, which represents less hydrogen bubbles than at high current densities.

The solubility product constants of Mn(OH)₂ and Co(OH)₂ are 2×10^{-13} and 5.92×10^{-15} , respectively. In solution of 0.50 M MnSO₄ with different CoSO₄, Co(OH)₂ can be formed when local pH reaches 6.6, 6.4, 6.2 in 0.05 M, 0.10 M CoSO₄ and 0.20 M CoSO₄ solutions, respectively, and Mn(OH)₂ forms at pH of 7.8. The formation of hydroxide implies the pH values have reached a pH range that a buffer cannot control. However, instead of finding Co(OH)₂ as expected, only Mn(OH)₂ was present in the coatings. There are two possible reasons for this,

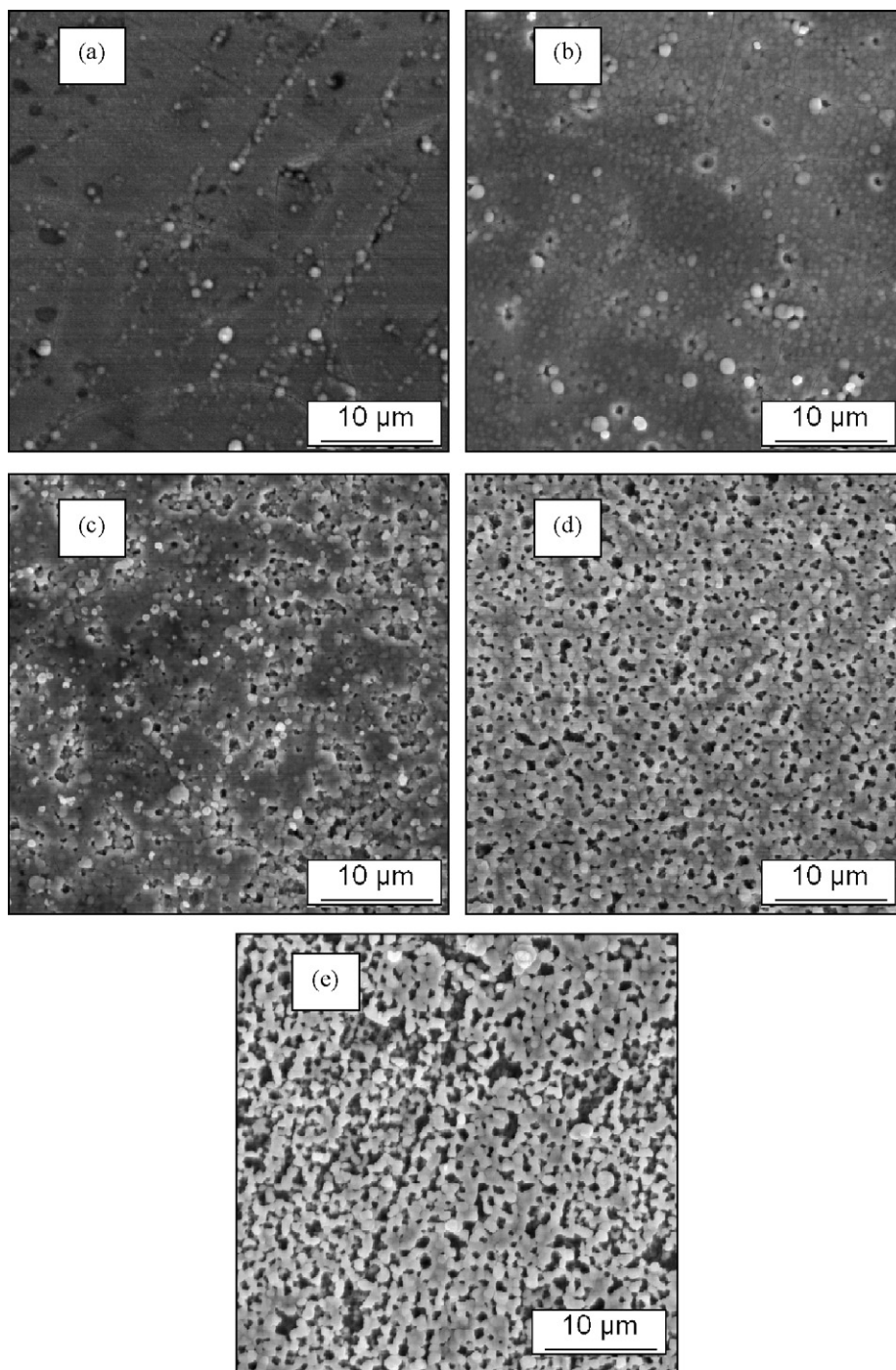
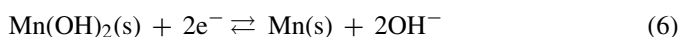


Fig. 9. Surface morphology of coatings with different current density in solution of 0.50 M MnSO_4 + 0.05 M CoSO_4 + 1.0 M H_3BO_3 + 0.70 M gluconate + 0.10 M $(\text{NH}_4)_2\text{SO}_4$ (pH 2.5). (a) 100 mA/cm²; (b) 150 mA/cm²; (c) 200 mA/cm²; (d) 250 mA/cm²; and (e) 300 mA/cm².

firstly, the low concentration of cobalt in the solution make it likely that cobalt has already reaches its diffusion control limit, thus making the concentration of cobalt at the surface where pH is highest very low near the cathode surface; so much higher pH value is required to form $\text{Co}(\text{OH})_2$. The other possibility is that $\text{Co}(\text{OH})_2$ may be reduced to cobalt directly by reaction (5) at -0.73 V vs. SHE. Although Mn could also be produced by reducing $\text{Mn}(\text{OH})_2$, the deposition potential is -1.55 V vs. SHE, more negative than that of $\text{Co}(\text{OH})_2$, even more negative

than Mn^{2+} reduction (-1.18 V vs. SHE).



In order to obtain compact and uniform Mn–Co coatings with lower hydroxide/oxide content, the hydrolysis of cobalt and manganese must be retarded or prevented. Chelating agent, especially gluconate, was used to stabilize cobalt and man-

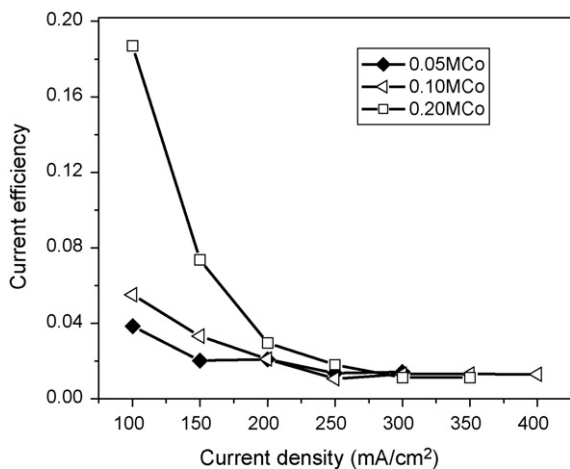


Fig. 10. Current efficiency as a function of cobalt concentration and current density in solution of 0.50 M MnSO₄ + 1.0 M H₃BO₃ + 0.70 M gluconate + 0.10 M (NH₄)₂SO₄ (pH 2.5).

ganese [15,17,19], which can always form more stable ligands with cobalt than with manganese as shown by the stability constants of the respective complexes [21]. Additionally, in the solution preparation procedures, cobalt was chelated with gluconate first before manganese sulfate was added. The addition of the chelating agent moves the reduction of cobalt to more negative potentials.

The structure of sodium gluconate is shown in Fig. 11. According to reference ([22]), Co²⁺ is present mainly as [Co(C₆H₁₁O₇)]⁺ complex, gluconate ion is attached to Co²⁺ by coordination through the carboxyl group and one of the adjacent hydroxyl groups. Addition of gluconate will reduce the free cation concentrations, therefore, the pH value for hydroxide formation is increased. After all the cobalt has been chelated, the rest of gluconate was able to chelate with Mn²⁺. If all the manganese and cobalt cations are chelated, no hydroxide could precipitate on the substrate surface during deposition, even if the pH excursion has out the range of pH buffer. However, considering the lower chelating effect of gluconate with manganese, it is important to add excessive amount of gluconate to make sure the chelation is complete. This is consistent with the

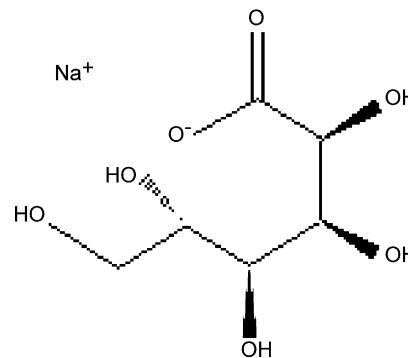


Fig. 11. Structure of sodium gluconate.

Table 3

Hydroxide formation in the base solution of 0.50 M MnSO₄ + 1.0 M H₃BO₃ + 0.1 M (NH₄)₂SO₄ (pH 2.5)

No.	CoSO ₄ (M)	Gluconate (M)	Current density (mA/cm ²)	Hydroxide	Extra gluconate (M)
1	0.10	0.20	100	Yes	-0.40
2	0.10	0.40	200	Yes	-0.20
3	0.05	0.70	300	No	0.15
4	0.10	0.70	400	No	0.10
5	0.20	0.70	200	Yes	0

data in Table 3, only solutions with excessive amounts of gluconate avoid hydroxide formation even at the current density of 300 mA/cm².

Comparing the Mn% in Fig. 8, Mn concentration in the solution of 0.10 M CoSO₄ solution is a slightly higher than that of 0.05 M CoSO₄ solution. This may correspond to extra gluconate in the solutions 0.15 and 0.10 M, respectively (Table 3). Higher amount of gluconate will reduce the free cations of Mn²⁺ in 0.50 M MnSO₄ solutions, therefore during deposition, deposition rate of Mn will be somewhat lower, resulting in lowering Mn concentration in the coating.

To summarize, excessive amount of gluconate guarantees all manganese and cobalt cations are be chelated, so little or no hydroxide was produced during deposition. By varying the cur-

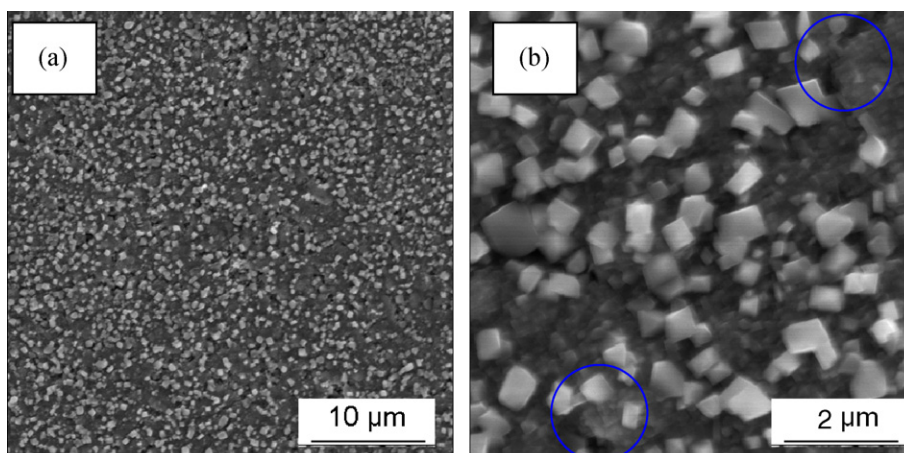


Fig. 12. Surface morphology of oxidized coating obtained at 250 mA/cm² in 0.05 M CoSO₄ solution (a) low magnification; and (b) high magnification.

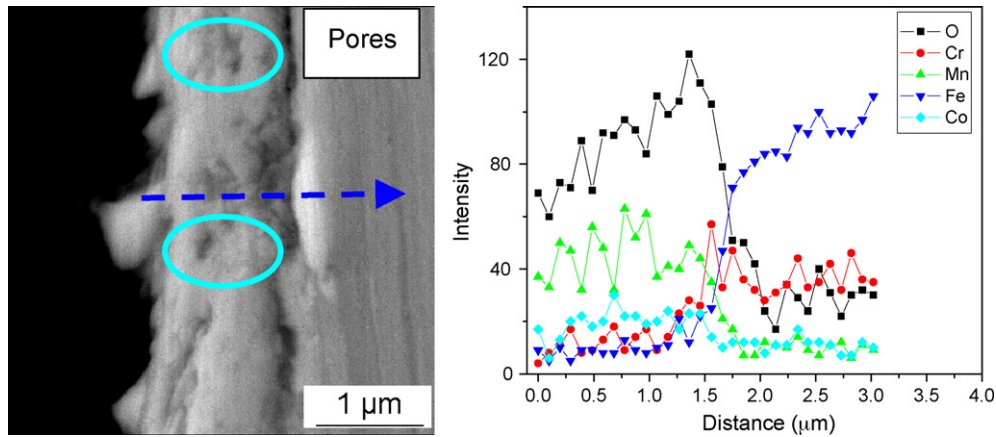


Fig. 13. Cross section and line scan of oxidized $\text{Mn}_{34}\text{Co}_{66}$ coating.

rent densities, coatings composition could be tuned to get the desired Mn–Co coatings.

3.5. Coating oxidation

The samples were oxidized at 900°C for 2 h. The SEM images as seen in Fig. 12 show the presence of numerous cubic structures, consistent with spinel formation. Also, compared with Fig. 9(d), it can be seen that the porosity has been significantly reduced, although not eliminated completely. Cross-section of oxidized sample, also displayed in Fig. 13, show the oxidized coating scale is around $1.5\ \mu\text{m}$, with some pores are shown in the coatings. However the pores do not appear to go through the whole thickness. An EDX line scan through the coating demonstrated that Mn content is higher than Co content, as well as having some chromium enrichment at the interface, consistent with the formation of a subscale of chromia or MnCr spinel. XRD pattern, Fig. 14, shows the presence of Mn_2CoO_4 , and a small amount of Cr_2O_3 and MnCr_2O_4 . Since coating is relatively thin, and Mn diffuses outward from the SS 430 substrate (Table 1) at 900°C [5], the coating is richer in Mn after oxidation than that of as deposited samples.

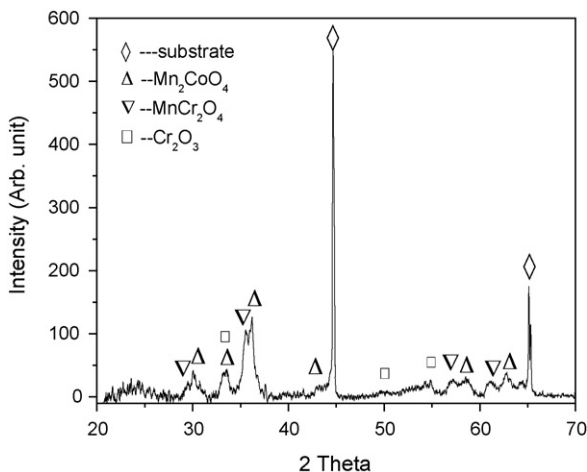


Fig. 14. XRD patterns of oxidized $\text{Mn}_{34}\text{Co}_{66}$ coating.

Therefore, thick coatings and reduced porosity will be helpful to form $\text{Mn}_{1.5}\text{Co}_{1.5}\text{O}_4$ spinel. Pulse plating has been regarded as better plating mode than DC plating, three parameters, the peak current density, the on-time and the off-time can be varied independently. Off time in pulse plating enables larger currents/voltages to be applied during the on time, the mass transfer limitation can be alleviated and resulting surface morphology and current efficiency is improved [23]. A review of the theory and practice of pulse plating is available [24], which can also be applied in our system. Therefore, our future will focus on improving the coating morphology, current efficiency and thickness by pulse plating.

4. Concluding remarks

In this research, a uniform, smooth Mn–Co alloys were successfully deposited on SS 430 substrate by DC electrodeposition. Polarization curves were used to characterize the four cathodic reactions and reaction potentials on substrate surface. The optimum electrolyte composition is $0.50\ \text{M}\ \text{MnSO}_4 + 0.10\ \text{M}\ \text{CoSO}_4 + 1.0\ \text{M}\ \text{H}_3\text{BO}_3 + 0.70\ \text{M}$ gluconate + $0.10\ \text{M}\ (\text{NH}_4)_2\text{SO}_4$. During deposition, in excessive gluconate solutions, Mn–Co alloys composition could be tuned by varying the current density. Coatings with Mn–Co around 1:1 could be obtained at the current density of $250\ \text{mA}/\text{cm}^2$, however porosity of the coatings also increases with current densities. The use of excessive gluconate in the deposition solution inhibits the formation of hydroxide and guarantees the deposition of continuous coatings. Oxidation of the alloy coatings decreases porosity such that no continuous pores penetrate through the coatings. Due to the Mn fast diffusion from the substrate and the generally thin coatings, Mn content becomes higher than cobalt in the coating after oxidation.

Acknowledgement

This project was funded as part of the Solid-State Energy Conversion Alliance (SECA) Core Technology Program by the U.S. Department of Energy's National Energy Technology Laboratory (NETL).

References

- [1] W.Z. Zhu, S.C. Deevi, *Mater. Sci. Eng. A* (2003) 227–243.
- [2] M. Han, S. Peng, Z. Wang, Z. Yang, X. Chen, *J. Power Sources* 164 (2007) 278–283.
- [3] J.W. Fergus, *Mater. Sci. Eng. A* 397 (2005) 271–283.
- [4] H. Kurokawa, C.P. Jacobson, L.C. DeJonghe, S.J. Visco, *Solid State Ionics* 178 (2007) 287–296.
- [5] S.P. Simner, M.D. Anderson, G. Xia, Z. Yang, L.R. Pederson, J.W. Stevenson, *J. Electrochem. Soc.* 152 (2005) A740–A745.
- [6] M. Burriel, G. Garcia, J. Santiso, A.N. Hansson, S. Linderoth, A. Figueras, *Thin Solid Films* 473 (2005) 98–103.
- [7] X. Chen, P.Y. Hou, C.P. Jacobson, S.J. Visco, L.C. De Jonghe, *Solid State Ionics* 176 (2005) 425–433.
- [8] M.R. Bateni, P. Wei, X. Deng, A. Petric, *Surface Coat. Technol.* 201 (2007) 4677–4684.
- [9] X. Deng, P. Wei, M.R. Bateni, A. Petric, *J. Power Sources* 160 (2006) 1225–1229.
- [10] M. Stanislowski, J. Froitzheim, L. Niewolak, W.J. Quadackers, K. Hilpert, T. Markus, L. Singheiser, *J. Power Sources* 164 (2007) 578–589.
- [11] Z. Yang, G. Xia, J.W. Stevenson, *Electrochem. Solid-State Lett.* 8 (2005) A168.
- [12] Z. Yang, G. Xia, S.P. Simner, J.W. Stevenson, *J. Electrochem. Soc.* 152 (2005) A1896.
- [13] C. Johnson, R. Gemmen, C. Cross, MS&T'06 Conference on Alloy Films Deposited by Electroplating as Precursors for Protective Oxide Coatings on Solid Oxide Fuel Cells Metallic Interconnect Materials, Cincinnati.
- [14] S.S. Abd El Rahim, M.A.M. Ibrahim, M.M. Dankeria, M. Emad, *Trans. IMF* 80 (2002) 105–109.
- [15] J. Gong, G. Zangari, *Mater. Sci. Eng. A* 344 (2003) 268–278.
- [16] A. Brenner, *Electrodeposition of Alloys*, vol. II, Academic Press, 1963.
- [17] K. Chen, G.D. Wilcox, *J. Electrochem. Soc.* 153 (2006) C634–C640.
- [18] J. Gong, G. Zangari, *J. Electrochem. Soc.* 151 (2004) C297–C306.
- [19] T. Cohen-Hyams, W.D. Kaplan, D. Aurbach, Y.S. Cohen, J. Yahalom, *J. Electrochem. Soc.* 150 (2003) 28–35.
- [20] F. Mangolini, L. Magagnin, P.L. Cavallotti, *J. Electrochem. Soc.* 153 (2006) 623–628.
- [21] A.E. Martell, R.M. Smith, *Critical Stability Constants*, Plenum Press, New York, 1974.
- [22] S.S. Abd El Rehim, M.A.M. Ibrahim, M.M. Dankeria, *J. Appl. Electrochem.* 32 (2002) 1019–1027.
- [23] D. Landolt, A. Marlot, *Surface Coat. Technol.* 169–170 (2003) 8–13.
- [24] J.-Cl. Puipe, F. Leaman (Eds.), *Theory and Practice of Pulse Plating*, AESF Soc., Orlando, FL, 1986.